ADVANCED FUNCTIONAL MATERIALS
www.afm-journal.de

Organic A-Site Cations Improve the Resilience of Inorganic Lead-Halide Perovskite Nanocrystals to Surface Defect Formation

*Clara Otero-Martínez, Junzhi Ye, Luca De Trizio, Luca Goldoni, Akshay Rao, Jorge Pérez-Juste, Robert L. Z. Hoye, Liberato Manna, and Lakshminarayana Polavarapu**

Lead halide perovskite nanocrystals (LHP NCs) are generally prone to surface defect formation during the purification process, resulting in a reduced photoluminescence (PL) quantum yield. The purification of LHP NCs using antisolvents leads to the detachment of surface atoms and ligandsin the form of alkylammonium-halides or A-carboxylates (A: Cs, methylammonium, MA, or formamidinium, FA. Currently, intense research is being carried out to improve the surface stability of LHP NCs using various long-chain organic ligands that strongly bind to the surface of NCs. Herein, the findings on the higher surface stability of hybrid ($MAPbBr_3$ and $FAPbBr_3$) LHP NCs compared to that of inorganic $CsPbBr_3$ NCs against purification with polar antisolvents are reported. It is discovered that the $CsPbBr_3$ NC surface stability can be enhanced (reaching that of hybrid perovskite NCs) by the incorporation of a small amount of MA or FA A-site organic cations into their lattice, corroborated by the evidence that the PL quantum yield of mixed A-cation $Cs_xFA_{1-x}PbBr_3$ and $Cs_xMA_{1-x}PbBr_3$ NCs remains unaffected after several purification cycles. It is hypothesized that this is attributed to hydrogen bonding between the organic A-site cations and the neighboring halides on the surface. These findings are not only fundamentally important but are also expected to have wide implications in the field of metal-halide perovskite optoelectronics.

1. Introduction

Lead halide perovskite (LHP) nanocrystals (NCs) have highly appealing properties for a variety of applications in next-generation optoelectronics.[1–5] These include narrow photoluminescence (PL) peaks, near-unity PL quantum yield (QY), long charge-carrier diffusion lengths, facile synthesis, and defect tolerance, among many others. These properties have made LHP NCs promising candidates for next-generation solar cells, light-emitting diodes (LEDs), quantum light sources, lasers, photodetectors, and photocatalysis.[1,6–8] All of these applications, in principle, require purified colloidal solutions without unreacted precursors and excess ligands present in them.

Typically, colloidal LHP NCs are stabilized by organic ligands such as a combination of long-chain alkylamine and acid ligands, in most cases oleylamine and oleic acid, which transform into the corresponding ionic species (e.g., oleylammonium (OLAm) and oleate (OL)) in the reaction

C. Otero-Martínez, J. Pérez-Juste, L. Polavarapu
Centro de Investigación en Nanomateriais e Biomedicina (CINBIO)
Department of Physical Chemistry
Materials Chemistry and Physics Group
Universidade de Vigo, Campus Universitario As Lagoas-Marcosende
Vigo 36310, Spain
E-mail: lakshmi@uvigo.es

J. Ye, R. L. Z. Hoye
Inorganic Chemistry Laboratory
Department of Chemistry
University of Oxford
South Parks Road, Oxford OX1 3QR, UK

The ORCID identification number(s) for the author(s) of this article can be found under https://doi.org/10.1002/adfm.202404399

DOI: 10.1002/adfm.202404399

J. Ye, A. Rao
Cavendish Laboratory
University of Cambridge
19 JJ Thomson Avenue, Cambridge CB3 0HE, UK

L. De Trizio
Chemistry Facility
Istituto Italiano di Tecnologia
Viao Morego 30, Genova 16163, Italy

L. Goldoni
Material Characterization Facility
Istituto Italiano di Tecnologia
Via Morego 30, Genova 16163, Italy

L. Manna
Nanochemistry, Istituto Italiano di Tecnologia
Via Morego 30, Genova 16163, Italy

medium.[9–15] The interaction of these two ligands with the surface of $CsPbBr_3$ NCs has been studied in detail and it was found that OLAm partially or fully replaces the Cs^+ ions while OL replaces the Br^- ions on the NC surface.[11,12,16–18] In addition, previous reports have demonstrated that the ammonium group of OLAm can form hydrogen bonds with the neighboring surface bromide ions.[11,12,19,15] Nevertheless, the interaction between these surfactants and the NC surface is electrostatic and, thus, highly dynamic in nature.[1,11–13] Therefore, excess ligands appear to be essential to maintain an equilibrium between the ligands that bind to the NC surface and those that are in the solution, and thus enable the colloidal stability of the NCs. However, the excess free ligands significantly hamper device applications, as they essentially behave as insulators. In addition, it is often difficult to prepare dry films in the presence of excess ligands, as most ligands have high boiling points. The LHP NCs can be effectively purified by precipitation through the addition of polar antisolvents, such as methyl acetate (MeOAc) or ethyl acetate.[20–22] However, this process significantly lowers the PLQY of the inorganic LHP NCs, as a fraction of the surface ligands are removed during the purification process, and even changes in morphology have been often observed.[23–27]. The decrease in PLQY has been attributed to the formation of trap states caused by the appearance of surface vacancies (mainly undercoordinated halide species) following the ligands detachment.[12,23–25,28,29] To overcome this, various in-situ and post-synthetic surface treatment strategies have been developed to obtain defect-free inorganic LHP NCs. In addition, different types of long-chain ligands with bi- and multi-functional groups have been exploited to stabilize the LHP NC surfaces against the purification process.[12,30,31]

Although the surface chemistry of LHP NCs with the ABX_3 crystal structure has been explored in inorganic systems (A = Cs), that of their hybrid analogs (A = MA or FA) has been rarely investigated. In general, the formation of large polarons in the hybrid systems provides a protective shield against traps and makes them more favorable for charge-carrier transport.[32–34] Furthermore, mixed A-site cation compositions have shown better device performance not only in thin films but also in NC systems.[35–37] Despite their interesting properties, the surface stability of hybrid LHP NCs against purification has been rarely investigated, but it is critical for improving their device performance.[38,39] Moreover, how the surface stability against purification is affected when both the organic and inorganic A-site cations are present in the same crystal structure is yet to be investigated. Therefore, it is important to understand the surface chemistry of mixed A-site cation NCs before developing new strategies to enhance their surface stability against purification. Especially, this step is vital for the development of LHP NC-based optoelectronic and photovoltaic devices, in which the surfaces play a crucial role in the device performance.[1]

In this work, we systematically studied the surface chemical stability of LHP NCs with different A-site cation compositions, including pure Cs-based, pure MA-based, pure FA-based NCs, along with mixed Cs-FA, and Cs-MA NCs, by studying the resilience of the NC surface to interactions with polar antisolvents during the purification steps. The colloidal NCs were washed several times with MeOAc and their optical properties (spectrally-resolved PL, PLQY, and PL lifetime) were analyzed before and after each washing step, and correlated with their surface characterization through nuclear magnetic spectroscopy (^{1}H-NMR) and X-ray photoelectron spectroscopy (XPS). We found that the hybrid compositions present superior surface stability compared to $CsPbBr_3$ NCs in terms of formation of a lower amount of defects caused by the detachment of surface ligands and halides. We find that the mixed A-site cation NCs with only 15% substitution of Cs^+ to MA^+ or FA^+ exhibit the same surface stability as the pure organic A-site NCs. Also, in contrast to mixed-halide systems, in which the halides tend to segregate into inhomogeneous domains after purifying with antisolvents, causing PL spectral shifts,[24] the treatment with antisolvent does not induce A-site cation segregation or any change in the optical properties.

2. Results and Discussion

2.1. Effect of Washing on the Optical Properties of LHP Nanocrystals

To study the influence of the type of A-site cation on the surface stability of LHP NCs against purification, we first synthesized pure $FAPbBr_3$, $MAPbBr_3$, and $CsPbBr_3$ NC by hot injection, using oleylamine and oleic acid as capping ligands, and octadecene as the solvent (see Experimental Section for more details).[1,2,40] Generally, LHP NCs are expected to have AX surface termination regardless of the A-site cation, as they were synthesized using primary alkylamine and carboxylate ligands in all cases.[18] The as-synthesized NCs were first separated from the crude reaction solution by centrifugation at 8 000 rpm without using any antisolvent to maintain a ligand-rich environment, as well as a fully passivated NC surface. The three $APbBr_3$ (A = Cs, MA, and FA) colloidal dispersions obtained after redispersing the NCs in toluene are named/referred to as "stock" solutions, and are the starting materials in the antisolvent-assisted washing experiments that will be described later (**Figure 1**a). The stock solutions were characterized by transmission electron microscopy (TEM), which showed that all three samples consist of cubic NCs having a size of between 9.1 and 10.8 nm, and a nearly-monodisperse size distribution (Figure 1b–d; Figure S1, Supporting Information). The emission properties (PL peak position and PLQY) of the three samples were studied before and after washing them twice with MeOAc antisolvent, as illustrated in Figure 1e–g. As depicted in Figure 1e and Figure S1 (Supporting Information), the as-synthesized $APbBr_3$ NCs exhibited narrow emission with peak maxima located at 515 nm (A = Cs and MA) and 530 nm (A = FA). Prior to NC washing, the stock solutions were systematically diluted to obtain $APbBr_3$ NC dispersions of similar concentration based on the optical density at the excitonic peak of the absorption spectra (see Figure S1, Supporting Information).[41] It is worth noting that the extinction coefficient of the three samples is considered similar because the optical transitions in LHPs are less dependent on the A-site cations and are mainly controlled by $[PbX_6]^{4-}$ octahedral units.[35] Eventually, the stock solutions were subjected to 2 cycles of washing using MeOAc (2:1 volume ratio of NC to antisolvent, Figure 1a). The washing process not only removes the free ligands in the colloidal solution but also accelerates ligand detachment from the surface of the NCs. The TEM images and the optical properties of the three samples before and

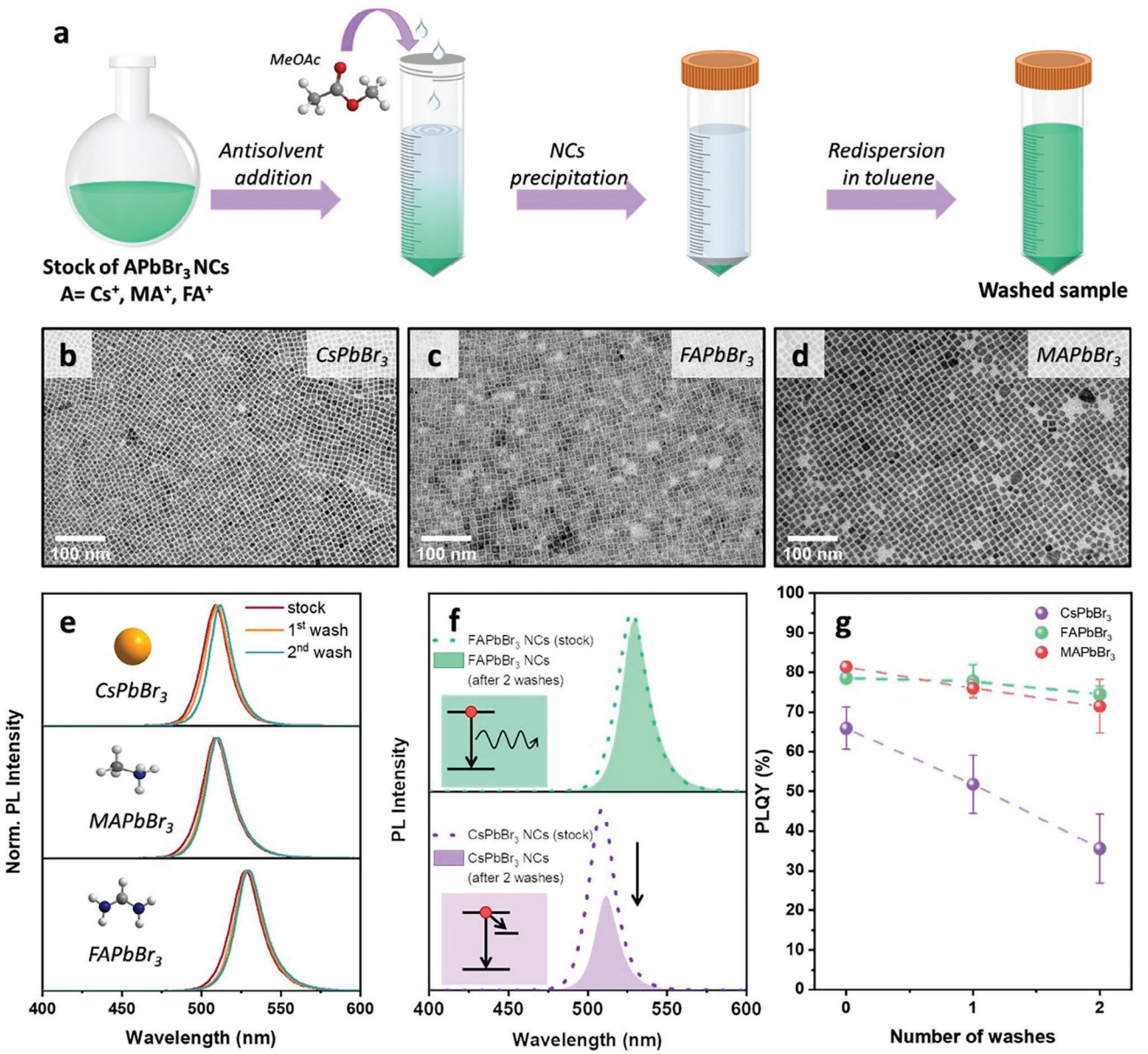

Figure 1. a) Illustration of the purification process with MeOAc of different A-site cation NCs stock solutions. b–d) TEM images of NCs with different A-site cations obtained from their stock solutions: $CsPbBr_3$ (b), $FAPbBr_3$ (c) and $MAPbBr_3$ (d). e) Normalized PL spectra of colloidal NC solutions with different A-site cations before and after washing (1st and 2nd). f) PL intensity of $FAPbBr_3$ before and after washing the NCs (top panel) and quenching of the PL intensity after $CsPbBr_3$ NC washing due to the formation of trap states (bottom panel). g) Variation of the PLQY with the number of washing steps for the different A-site cation NCs with respect to the stock solution. The values shown in the plot correspond to the average result and the corresponding error bar after reproducing the experiment 5 times.

after each washing cycle are shown in Figure 1b–g and Figures S1 and S2 (Supporting Information).

It was found that the washing of NCs did not lead to a significant shift in the PL peak position or changes in spectral shape (Figure 1e), suggesting that the morphology of the washed NCs remained unaltered after treating them with the antisolvent, as there was no obvious etching or phase change during the purification process (Figure S2, Supporting Information). In line with previous studies,[10,12,25] although the PL peak position of $CsPbBr_3$ NCs remained unchanged after the two washing cycles, a significant reduction in PL intensity with each washing cycle was observed. The PLQY of the $CsPbBr_3$ NCs drastically decreased to ≈50% of its initial value after two cycles of washing (Figure 1f,g; Table S1, Supporting Information). On the other hand, the PLQY of hybrid perovskite NCs (A = FA and MA) after two washing cycles was reduced by only ≈15% (Figure 1g; Table S1, Supporting Information). Moreover, the initial stock solutions of the hybrid colloidal perovskite NCs exhibit higher PLQY as compared to the $CsPbBr_3$ NCs stock solution used for obtaining mixed A-site cation systems. It is worth mentioning

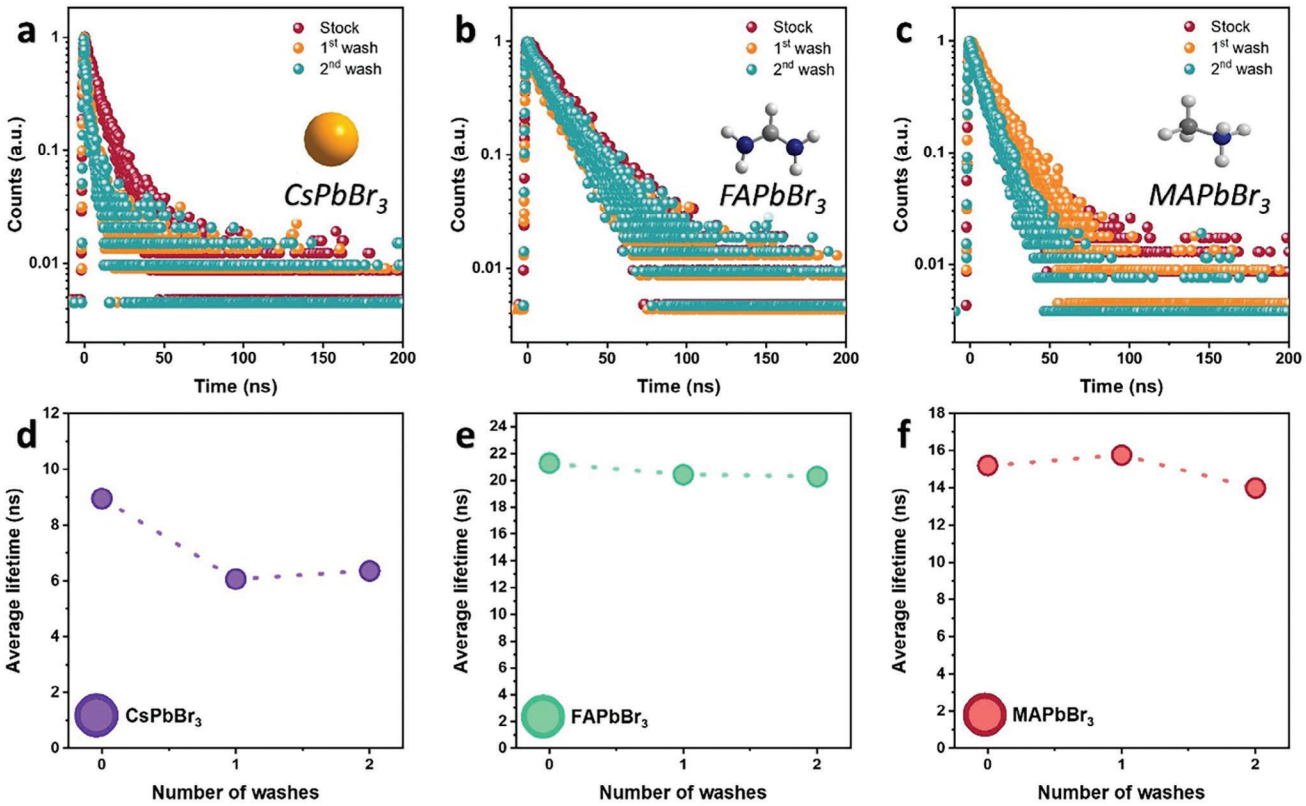

Figure 2. a–c) PL lifetime decays before and after the NC washing for the different A-site cation compositions: $CsPbBr_3$ NC (a), $FAPbBr_3$ (b), and $MAPbBr_3$ (c). d,e) Average lifetime before and after the NC washing for the different A-site cation compositions: $CsPbBr_3$ (d), $FAPbBr_3$ (e), and $MAPbBr_3$ f) obtained with a bi-exponential model.

that the experiments were repeated several times, and the PLQY trend of the stock solutions and the effect of washing remained the same in all trials. The TEM images of the colloidal NC solutions before and after the washing steps confirmed that antisolvent treatment did not affect the morphology of the NCs for the three samples (Figure S2, Supporting Information). Based on this, we anticipate that the differences in the optical properties of the NCs are mainly due to changes in their surface passivation (ligands density and surface halide vacancies) upon purification. To probe the differences in the three systems, first, we investigated the time-resolved PL decay of the three colloidal solutions before and after washing (see **Figure 2**). The average PL lifetime of the initial stock solutions of hybrid perovskite NCs is found to be longer than $CsPbBr_3$ NCs. (Table S1, Supporting Information; Figure 2a,d). Interestingly, the PL decay of the $CsPbBr_3$ NCs became significantly faster (decreased from 8.95 to 6.35 ns) after washing (Table S1, Supporting Information; Figure 2a), while the PL lifetime of the hybrid perovskite NCs (≈20 and 15 ns for $FAPbBr_3$ and $MAPbBr_3$ NCs, respectively) remained unaffected after two washing cycles (Figure 2b–d, Figure S2c, Table S1, Supporting Information). The changes in the PL lifetime of the three NCs upon washing can be correlated with the PLQY data. For $CsPbBr_3$ NCs, the decrease in PLQY and shortening of PL decay suggests the increase of non-radiative decay upon washing, which is likely due to the formation of surface traps by the detachment of surface ligands and halides during the washing process. On the other hand, the PLQY and PL lifetimes of hybrid NCs are less affected by the washing process. These results suggest two possible scenarios: either a higher defect tolerance in the hybrid compounds, or differences in the defect formation energy for different A-cation compositions by variations in the chemical stability of the surfaces.

2.2. Effect of Washing on the Surface Composition of $APbBr_3$ NCs (A = Cs, FA, and MA)

To understand the effect of the antisolvent-assisted purification on the surface chemistry of NCs with different A-site cations (Cs and FA), we investigated their surface composition as well as their ligand density through NMR spectroscopy after two washing cycles (**Figure 3**). First, to study the ligand binding on the NCs surface, we acquired ^{1}H NMR spectra of the washed $CsPbBr_3$ and $FAPbBr_3$ colloidal dispersions in toluene-d_8 (Figure 3a, violet and green spectra; Figure S4a, Supporting Information, red spectrum) and compared them with ^{1}H NMR spectra of the free ligands (OLAm & OL) (Figure S3, Supporting Information). The ^{1}H NMR spectrum of the NCs with different A-site cation compositions exhibits resonance peaks broader than those of the free ligands in the same solvent. This suggests that the ligands dynamically interact with the NC surface, consistent with previous reports.[11,42]

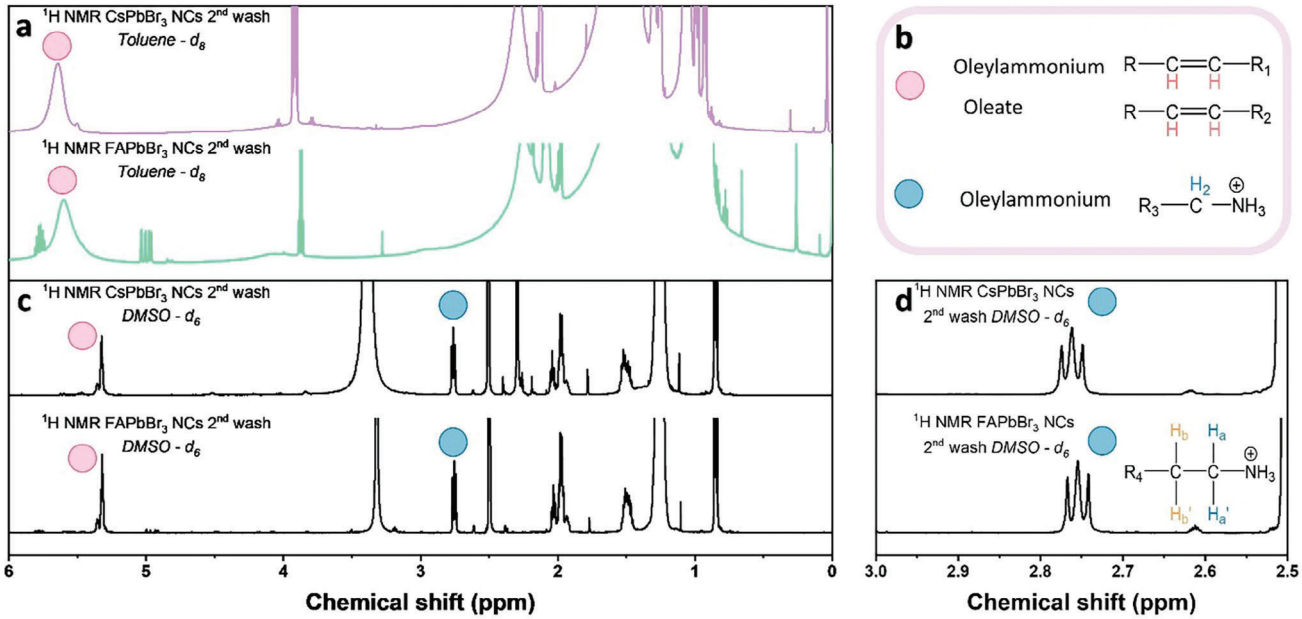

Figure 3. a) ^{1}H NMR spectra of colloidal solutions of $CsPbBr_3$ (top spectrum, violet) and $FAPbBr_3$ (bottom spectrum, green) NCs after 2 cycles of washing with MeOAc and dispersed in toluene-d_8. b) Diagnostic ligand peak assignment: the pink circle corresponds to the double bond ^{1}H of both OL and OLAm ligands. The blue circle corresponds to protons in position α to a nitrogen atom, which is a signature of OLAm. c) ^{1}H NMR spectra obtained after dissolving $CsPbBr_3$ (top spectrum, black) and $FAPbBr_3$ (bottom spectrum, black) NCs in DMSO-d_6. The spectra in the 2 different solvents (toluene-d_8 and DMSO-d_6), show the differences in the peak broadening when the ligands are bound to the surface (toluene-d_8 spectra) or free in the solution (DMSO-d_6 spectra). d) Enlarged ^{1}H NMR spectral region, showing the pseudo-triplet signal attributed to the protons in position α to the nitrogen atom.

Besides the broadening of the peaks, the ligand signals in the ^{1}H NMR spectrum of the NCs appear at different chemical shifts compared to the resonances obtained in the ^{1}H NMR spectrum of free ligands (Figure S3, Supporting Information). This is noteworthy for the double bond peak of both ligands (OLAm & OL), which appears at ≈5.6 ppm for the ligands bound to the surface of the NCs and at ≈5.4 ppm for free ligands (Figure 3a; Figures S3 and S4, Supporting Information, peaks with pink circles). Interestingly, the 2D ^{1}H-^{1}H NOESY spectra of the hybrid NC ($FAPbBr_3$ and $MAPbBr_3$) colloidal solutions in toluene-d_8 (Figures S5 and S6, Supporting Information) show negative (red) NOE cross peaks. This is typical for species with a correlation time (τ_c) longer than that of free ligands, which instead exhibit positive (blue) NOE cross peaks (Figure S7, Supporting Information). Hence, ligands acquired the slow tumbling regime of the NCs when binding or temporarily interacting with the NC surface.[43] These results provide two important insights: on the one hand, the OLAm ligands interact with the A-site cations at the surface, which proves the ligand binding to the NC; on the other hand, it confirms the presence of organic A-site cations (MA or FA) partially covering the A-sites on the surface of the NCs.

Next, the ligand densities on the different NC surfaces are calculated after two cycles of washing. This is to study the influence of A-site composition on ligand detachment and the origin of trap formation on the NC surfaces upon washing with polar antisolvents. To quantify the density of surface OLAm & OL, the colloidal NC solutions in toluene-d_8 were dried and subsequently dissolved in deuterated dimethyl sulfoxide (DMSO-d_6), leading to the release of ligands in solution. The broad signal at ≈5.6 ppm that corresponds to the saturated double bond returns a well-defined multiplet at 5.3 ppm, typical of a free ligand in solution (Figure 3a; Figure S4, Supporting Information).Similarly, the protons in position α to nitrogen of the oleylammonium (H_a & H_a'), appear as a triplet at 2.75 ppm, which can be identified and quantified (Figure 3b,c). The ligand concentration in the solution is determined by the PULCON method[47] using a 5 mM dimethylsulfone solution in DMSO-d_6, as the external reference standard, and the data is summarized in Table S2 (see Supporting information for more details). The concentration of both ligands ([OLAm + OL]) is measured by using the double bond signal resonances at ≈5.3 ppm, while the concentration of OLAm ([OLAm]) alone is quantified from the resonances at ≈2.75 ppm. Finally, the concentration of OL ligands ([OL]) is calculated from the difference between the concentrations of both ligands together and the OLAm alone ([OL] = [OLAm + OL] – [OLAm]). Interestingly, we find that the hybrid systems show a significantly higher ligand density compared to that of $CsPbBr_3$ NCs after the 2nd washing step with MeOAc. The $CsPbBr_3$ NCs have a total ligand density of 2.2 ligands per nm^2, with only 10% being OL ligands and the rest being OLAm ligands. Surprisingly, $FAPbBr_3$ and $MAPbBr_3$ NCs exhibit not only a higher total ligand density (3.8 and 4.38 ligand per nm^2 respectively) but also different OLAm/OL ratios compared to $CsPbBr_3$: in the case of $FAPbBr_3$ NCs, the ligand composition is 23% OL and 77% OLAm, while in the case of $MAPbBr_3$ NCs the composition is 48% OL and 52 OLAm. The ligand density results suggest that the washing process led to the more efficient detachment of ligands from the surface of $CsPbBr_3$ NCs compared to that of hybrid perovskite NCs. We anticipate that this is most likely due to weaker ligand-surface interactions in $CsPbBr_3$ NCs compared to $FAPbBr_3$ and $MAPbBr_3$ NCs. More-

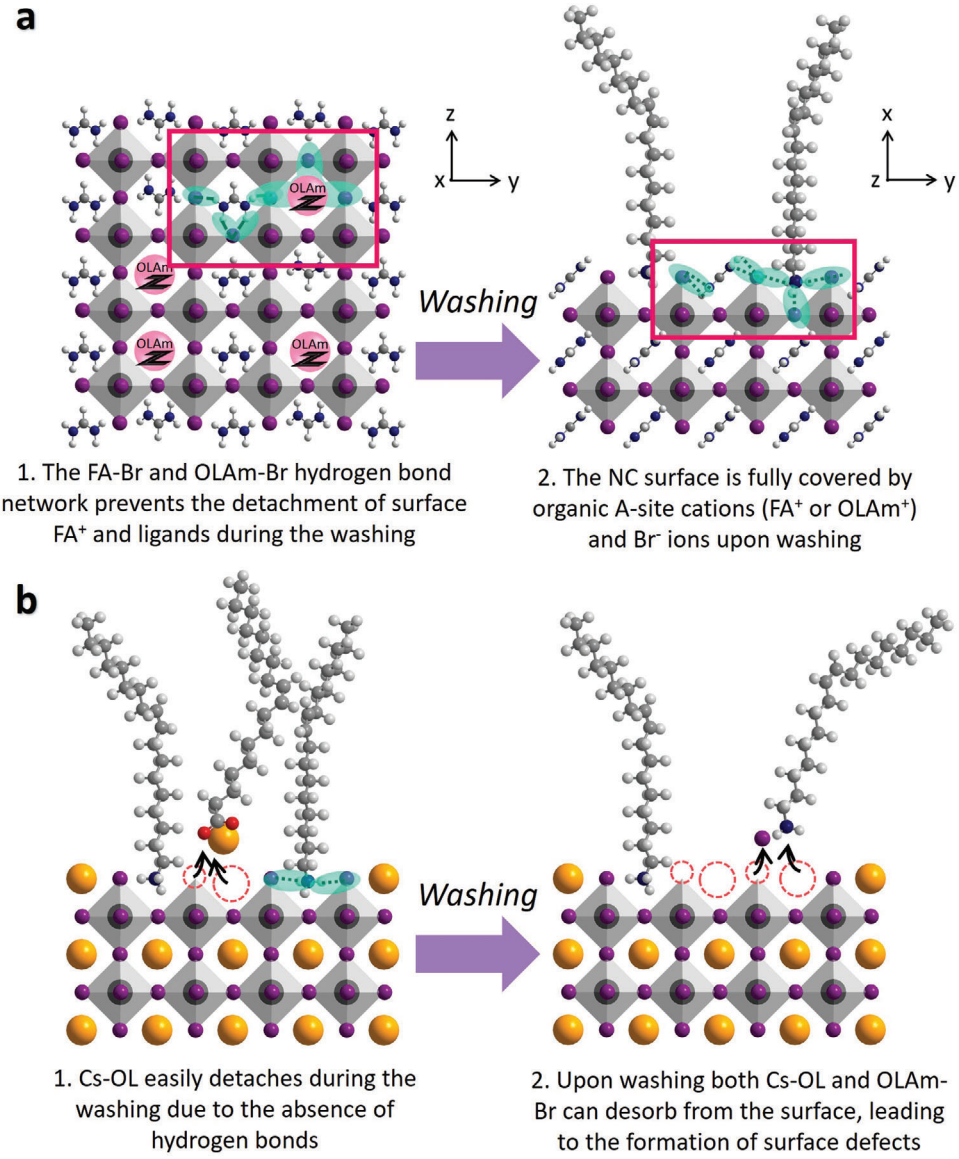

Figure 4. Schematic illustration of the antisolvent effect on $FAPbBr_3$ NCs a) and $CsPbBr_3$ NCs b). In the case of $FAPbBr_3$ NCs (a), the OLAm ligands and FA cations establish H-bonds with the neighboring bromides (step 1) that prevent the detachment of FA and OLAm during washing (step 2). The absence of H-bonds in the case of $CsPbBr_3$ (b) causes the detachment of Cs-OL, leading to the formation of A-site and X-site vacancies (step 1), and the consequent detachment of OLAm, along with the formation of halide vacancies (step 2).

over, the OLAm ligand would detach in the form of an OLA-Br complex, forming a pair of A-site and Br vacancies, to maintain charge neutrality.[29,45] Furthermore, the relative Br atomic ratio of the inorganic and hybrid perovskite NCs before and after washing them were determined by XPS (Figure S8, Supporting Information). The results show that the Br/Pb ratio on the surface of $FAPbBr_3$ and $MAPbBr_3$ NCs remains almost unaltered (69% and 71% respectively) after washing the NCs twice (Figure S8, Supporting Information, middle and bottom panel), while it decreased from 71.7% to 67.6% for $CsPbBr_3$ NCs (Figure S8, Supporting Information, top panel). Although this decrease is quite small, the decreasing trend with the number of washing cycles suggests the formation of more Br vacancies in $CsPbBr_3$ NCs than in $FAPbBr_3$ and $MAPbBr_3$ NCs (Figure S8, Supporting Information).

To explain the lower tendency for the formation of surface defects on hybrid LHP NCs compared to that of $CsPbBr_3$ NCs upon the washing-induced detachment of ligands and Br atoms, we postulated different chemical stabilities for the two surfaces, as illustrated in **Figure 4**. In the case of hybrid systems, the organic A-site cations can interact with the neighboring Br ions, thus resulting in higher defect formation energy than for the all-inorganic NC system.[19] In addition, the ligands interact more strongly with the hybrid NC surface than with the all-inorganic NC surface because of the hydrogen bonding between the A-site cations and the neighboring Br atoms on the surface of NCs, as

explained in the following. In the case of $CsPbBr_3$, let us assume that the washing experiments were performed on an ideal cubic system with A-Br/OL termination and no surface vacancies (here, A = Cs or ligand). The washing process results in the detachment of ligands and surface atoms from the $CsPbBr_3$ NCs, as illustrated in Figure 4b. First, a Cs-cation from the surface is desorbed in the form of a Cs-OL complex, which results in the formation of A-site and Br vacancies (Figure 4a). Second, the removal of Cs-OL from the surface will have a significant effect on the ligand binding. As soon as the A-cation and Br vacancies are generated, the overall hydrogen bond (H...Br) network that confers the stability to the NC surface weaken. This leads to a reduction in the binding energy of the ligand with the NC surface and thus facilitates the detachment of OLAm, resulting in the formation of a second pair of halide vacancies (Figure 4b). Thus, the washing process in $CsPbBr_3$ NCs generates more Br vacancies and can induce a new cycle of ligand detachment, which results in a significant reduction of PLQY as evidenced by optical measurements. On the other hand, in the case of hybrid systems, the organic A-site cation (FA and MA) could form hydrogen bonds with the neighboring Br atoms along with ionic interactions with the surface of NCs, as shown in Figure 4a. This makes the surface of hybrid perovskite NCs tolerant to the antisolvent-induced detachment of A-site cations (including ligands) and Br atoms. We also find that the higher density of OLAm ligands and A-site cations on the hybrid surface can also help to retain the OL ligands, which explains why the total calcualted density of OL ligands was 23% and 48% on the surface of $FAPbBr_3$ and $MAPbBr_3$ NCs, whereas the ligand density was only 10% for $CsPbBr_3$ NCs (Table S2, Supporting Information). According to the literature, in the presence of primary alkylamines, like OLAm, the OL ligands cover the surface of NCs by forming ion pairs with OLAm or A-site cation.[12,13,18] Therefore, a higher density of A-site cations or OLAm ligands on the NC surface could help retain the OL ligands covering the NC surface through ion pair interactions.

2.3. Surface Stability of Mixed A-Site Cation Systems Against Washing

As the hybrid perovskite NCs exhibit superior surface stability over their inorganic counterparts, we then investigated mixed A-site cation compositions ($Cs_xFA_{1-x}PbBr_3$ and $Cs_xMA_{1-x}PbBr_3$) to determine how their surface stability compares to pure inorganic and hybrid perovskite NCs. First, stock solutions of colloidal $Cs_xFA_{1-x}PbBr_3$ NCs were synthesized by interparticle A-site cation exchange or direct A-site cation exchange reactions, as illustrated in **Figure 5**a.[35,46] In the first case, different volumes of $CsPbBr_3$ and $FAPbBr_3$ colloidal stock solutions with the same NC concentration were mixed in different ratios in order to obtain the desired Cs/FA stoichiometry in the mixed A-site cation NCs (See Experimental Section for more details).[46] The mixed A-cation compositions were obtained through the A-cation cross-exchange reaction between the two A-site cation compositions ($Cs^+ \rightarrow FAPbBr_3$ and $FA^+ \rightarrow CsPbBr_3$). It is worth noting that all A-site cation ratios mentioned here are approximate, and are based on the assumption that the $APbBr_3$ NCs with the same size and concentration will have similar optical density near the band-edge regardless of the A-site cation composition. This is because the bandgap in lead halide perovskite NCs is dominated by lead-halide interactions, while the A-site cation only has minor contributions. Upon mixing $CsPbBr_3$ and $FAPbBr_3$ NCs, a new PL peak emerges in between the PL peaks of pristine $CsPbBr_3$ and $FAPbBr_3$ NCs, as shown in Figure 5b and Figure S9 (Supporting Information), confirming the formation of a mixed A-site cation composition. The PL peak position of the mixed A-site cation system depends on the ratio between Cs and FA. Thus, mixed A-site cation $Cs_xFA_{1-x}PbBr_3$ colloidal NCs with different Cs/FA ratios were prepared to study their surface stability and optical properties before and after washing with antisolvent, and the data is depicted in Figure 5c. First, we noticed a dramatic improvement in the PLQY upon the incorporation of FA into the $CsPbBr_3$ NC lattice. The PLQY of the $Cs_xFA_{1-x}PbBr_3$ NCs gradually increases with increasing the FA concentration until it reaches ≈15% of the total A-site cation concentration, and then it saturates at ≈80%, which is the PLQY of pure $FAPbBr_3$ NCs (Figure 5c). Then, the mixed A-site cation $Cs_xFA_{1-x}PbBr_3$ NCs solutions were subjected to the same cycles of purification as for the pure A-site cation compositions discussed above. Remarkably, the differences in the PLQYs of the mixed A-site cation colloidal NCs before and after washing gradually decrease with increasing the FA concentration (Figure 5c). This tendency continues until the NC composition reaches ≈$FA_{0.15}Cs_{0.85}PbBr_3$. From this point, the mixed A-site cation systems exhibit PLQY values as high as those of the pure hybrid systems regardless of the A-site cation composition, and the PLQY did not vary significantly after two washing cycles (Figure 5c). Despite the domination of Cs ions in the crystal lattice of the mixed A-site cation composition system, they exhibit surface stability as high as pure hybrid perovskite NCs against antisolvent-induced defect formation. After the threshold of ≈15% FA in the A-site ($FA_{0.15}Cs_{0.85}PbBr_3$ NCs), the surface of mixed A-site cation NCs is as tolerant as the surface of pure hybrid NCs against exposure to polar antisolvents. These results are very exciting, since the surface of $CsPbBr_3$ is exceptionally stable against purification just with 15% FA incorporation in the lattice, and such stability has been previously achieved by modifying the surface chemistry with multifunctional ligands.[15,47–58] Importantly, analogous studies (PLQY vs a number of washing cycles, and XRD) were performed on $Cs_xMA_{1-x}PbBr_3$ NCs synthesized by interparticle A-site cation exchange, and the results are similar to that of $Cs_xFA_{1-x}PbBr_3$ NCs (Figure S10, Supporting Information). The mixed A-site cation $Cs_xMA_{1-x}PbBr_3$ compositions exhibit PLQYs (≈70%), similar to that of pure $MAPbBr_3$ NCs, and are significantly higher than that of $CsPbBr_3$ NCs (≈50%) (Figure S10, Supporting Information). In addition, the PLQY of the $Cs_xMA_{1-x}PbBr_3$ NCs is less affected by the number of washing cycles as compared to that of pristine $CsPbBr_3$ NCs, and the $Cs_xMA_{1-x}PbBr_3$ NCs follow the same trend as pure $MAPbBr_3$ NCregarding the PLQY versus number of washing cycles (Figure S10, Supporting Information). These results suggest that both MA and FA can effectively passivate and stabilize the surface of $CsPbBr_3$ NCs. In addition, the surface composition stability of both $Cs_xFA_{1-x}PbBr_3$ and $Cs_xMA_{1-x}PbBr_3$ NCs was tested by XPS (Figures S11–S13, Supporting Information) with a typical fitted XPS spectra for Pb 4f and Br 3d is shown in Figure S11 (Supporting Information). By comparing the Br relative atomic ratio before and after the washing to the pure $APbBr_3$ NCs, we observe that both mixed A-site cation compositions show a smaller

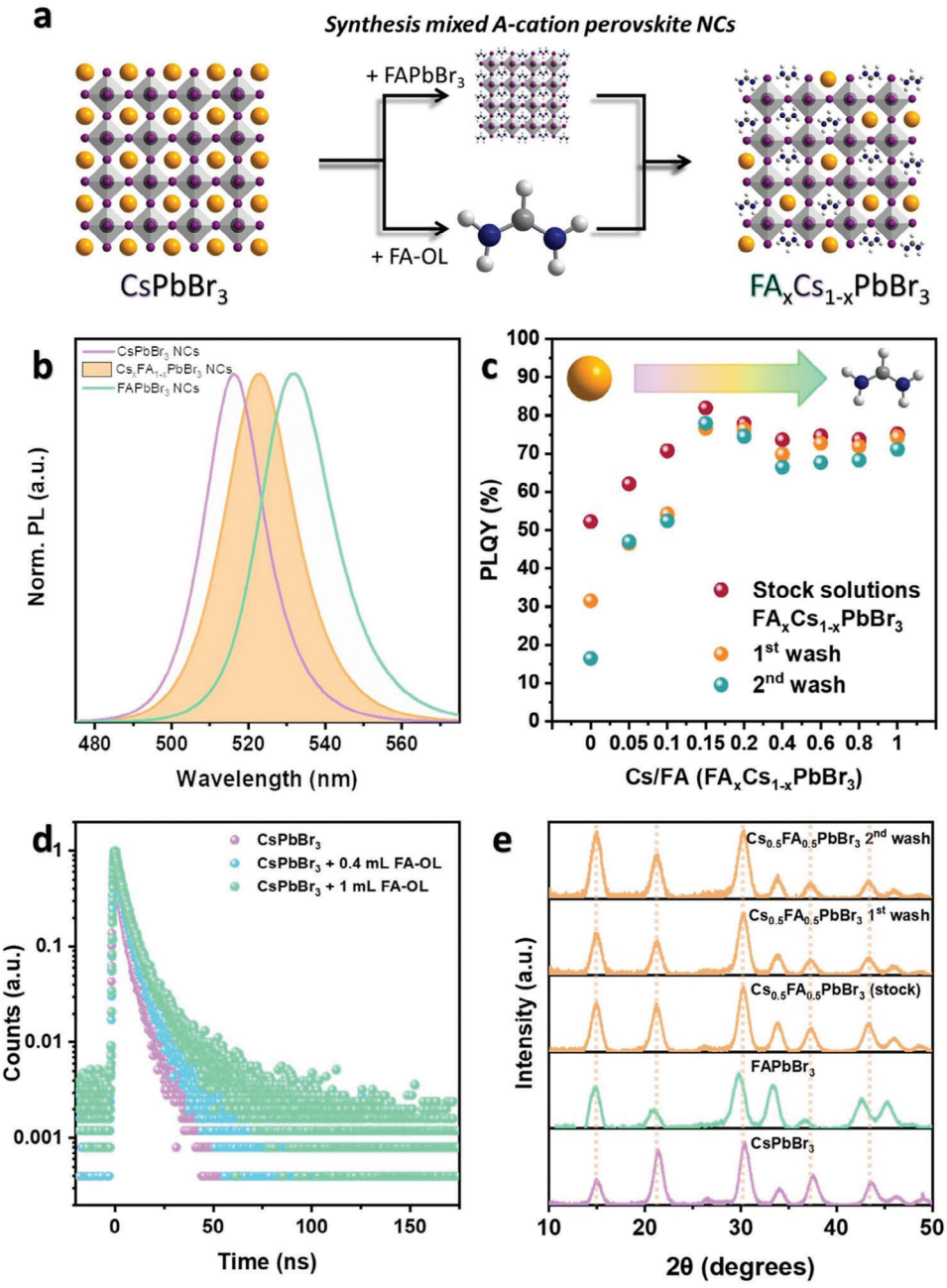

Figure 5. a) Schematic illustration of A-site cation exchange and interparticle A-site cation exchange reactions employed to obtain the mixed A-site cation NCs. b) PL spectra of $CsPbBr_3$, $FAPbBr_3$ NCs (unfilled curves), and $Cs_xFA_{1-x}PbBr_3$ NCs (filled curve). The relative PL shifts of the solutions reflect the A-site cation composition. c) PLQY values before and after the washing with MeOAc of colloidal dispersions of pure $CsPbBr_3$, $FAPbBr_3$, and mixed $Cs_xFA_{1-x}PbBr_3$ with different Cs/FA ratios. d) PL lifetime decays of $CsPbBr_3$ and $Cs_xFA_{1-x}PbBr_3$ NCs obtained by A-site cation exchange from $CsPbBr_3$ NCs. e) XRD diffraction patterns of pure $CsPbBr_3$ NCs $FAPbBr_3$ NCs after 1 wash and mixed $Cs_{0.5}FA_{0.5}PbBr_3$ NCs after several washes.

decrease of the Br atomic ratio, thus a lower trap formation ratio compared to that of pure A-cation compositions.

These results suggest that the FA cations are incorporated into the lattice of $CPbBr_3$ first by replacing the Cs atoms on the surface,[62] and thus resulting in a pure hybrid perovskite-like surface with similar chemical stability against purification. After a threshold concentration, the FA cations penetrate into the lattice, and they do not contribute to the additional surface stability. Furthermore, we confirmed the enhancement of the surface stability of $CsPbBr_3$ NCs through the incorporation of FA cations into the lattice by direct A-site cation exchange reaction (Figure 5a). In this case, a small volume of a FA-OL solution was added to a $CsPbBr_3$ NC pristine solution in toluene. After 5 min of stirring at room temperature the extinction and PL spectra were acquired (Figure S14a, Supporting Information), showing a 3 nm redshift in the absorption band-edge and the PL emission.

The PLQY of $CsPbBr_3$ NCs increased from ≈55 to ≈80% upon the addition of FA (see Figure S14b, Supporting Information), and the results are in accordance with the samples prepared by interparticle A-site cation exchange. In addition, the PLQY values of this mixed A-site cation system decrease only from ≈80% to ≈75% after two washing cycles (Figure S14b, Supporting Information). On the other hand, time-resolved PL decay measurements revealed that the addition of increasing volumes of FA-OL solution to the $CsPbBr_3$ NCs pristine solution results in a slower PL decay dependent on the FA concentration in the NCs, as is shown in Figure 5d. The increase of PLQY and the enhanced PL lifetime indicate the reduction of nonradiative decay because of trap state passivation upon the addition of FA to $CsPbBr_3$ NCs. Thus, the mixed A-cation systems with a threshold concentration of FA exhibit high PLQY and high surface stability against purification while there is only a small redshift in the PL peak position.

To probe the phase stability and robustness of the mixed A-site cation NCs against washing cycles, XRD diffraction patterns of the NCs were acquired after several washes with antisolvent. It is well-known that mixed halide systems suffer from the etching of surface atoms and spectral shifts after washing with antisolvent.[23,25] We acquired the XRD patterns of the mixed A-site cation system (≈$Cs_{0.50}FA_{0.50}$ and ≈$Cs_{0.50}MA_{0.50}$) after several washes and compared them with those of pure A-site cation samples (Figure 5e; Figure S15, Supporting Information). The diffraction pattern of $CsPbBr_3$ NCs shows the typical features of the orthorhombic phase whereas the XRD of $FAPbBr_3$ and $MAPbBr_3$ match with cubic crystal structure, and these are in agreement with previous reports.[60,61] On the other hand, the two mixed A-site cation systems exhibit a distortion of the lattice due to the octahedral tilting but are not as significant as for pure $CsPbBr_3$ NCs (Figure 5e; Figure S15, Supporting Information). As expected, the position of the diffraction features of the mixed A-site cation systems appear in between those of the pure A-site cation (Cs and FA; Cs and MA) lattices due to intermediate lattice spacing caused by the alloying of Cs with FA (see Figure 5e) and Cs with MA (Figure S15, Supporting Information). It is worth mentioning that in the case of the Cs-MA system, the shifts are smaller due to small differences in lattice spacing as compared to that of CA-FA systems. Moreover, after three washing cycles the diffraction features of the mixed A-cation NC sample remain unchanged. Furthermore, the patterns do not show any signs of peak splitting (indicative of two-phase coexistence) or any shift (indicative of phase transition), confirming that the A-site cation composition maintains constant, and the washing process does not induce A-site cation segregation.

3. Conclusion

In conclusion, we have demonstrated that the hybrid perovskite NCs ($FAPbBr_3$ or $MAPbBr_3$) exhibit better resilience to surface defect formation than their inorganic counterpart ($CsPbBr_3$). These defects are likely to form as a consequence of the interactions of the NC surface with polar antisolvents during theri purification, which is a mandatory step in the fabrication of NC-based optoelectronic devices. The formation of trap states in $CsPbBr_3$ NCs is evidenced by the decrease of the PLQY and the fastening of time-resoled PL lifetime. However, $FAPbBr_3$ and $MAPbBr_3$ NCs maintain their initial optoelectronic properties even after several washing cycles. The surface characterization of purified NCs of different A-site cation systems revealed that the ligand density is higher in hybrid systems, whereas $CsPbBr_3$ not only shows lower ligand density but also a reduction of the Br/Pb ratio. We attribute this to the stronger binding of the FA to the neighboring bromide ions through hydrogen bonds, which prevents the desorption of FA and Br ions and the consequent ligand detachment. Surprisingly, the $CsPbBr_3$ NCs exhibit the same surface stability as the hybrid systems upon the incorporation of a small amount (≈15%) of organic A-cation into the lattice. This is due to the accumulation of the added organic cations on the surface of $CsPbBr_3$ NCs, leading to a stabilization of the surface that mimics the case of pure hybrid systems. The XRD analysis after several washing cycles confirms that the mixed A-site cation LHP NCs do not suffer from cation segregation during the purification process, and the composition and crystallinity remain unchanged. Thus, the mixed A-cation systems possess the combined features, that is, higher stability against temperature and moisture that comes from the inorganic part and an improved surface stability stemming from the organic part. Therefore, we anticipate that there is a huge room for improving optoelectronic performance along with higher stability by A-cation engineering.

4. Experimental Section

Materials: Cesium carbonate (Cs_2CO_3, 99,9%), formamidine acetate salt ($CH_4N_2{\cdot}C_2H4O_2$, 99%), methylamine (CH_3NH_2, 2 M solution in tetrahydrofuran, THF), lead (II) bromide ($PbBr_2$, >98%), benzoyl bromide (97%), 1-octadecene ($C_{18}H_{36}$, 90%) oleic acid ($C_{18}H_{34}O_2$, 90%), oleylamine ($C_{18}H_{37}N$, 70%), methyl acetate (CH_3COOCH_3, 99%), toluene (C_7H_8, <99.8%), deuterated dimethyl sulfoxide-d_6 ($(CD_3)_2SO$,) and deuterated toluene-d_8 ($C_6D_5CD_3$, 99.95%) were purchased from Merck. All chemicals were used without further purification.

Nanocrystals Synthesis: $CsPbBr_3$, $FAPbBr_3$, and $MAPbBr_3$ NCs were synthesized following previously reported procedures with slight modifications.[2,40,61]

Preparation of a Stock Solution of Cesium-Oleate (Cs-OL): In a typical synthesis, 407 mg of Cs_2CO_3 (1.25 mmol) and 1.25 mL of oleic acid (3.5 mmol) were added to 20 mL of 1-octadecene in a 50 mL sample vial. The resulting mixture was heated at 150 °C under stirring until the salt was completely dissolved. The Cs-oleate complex generally precipitates at room temperature, however, it could be easily dissolved again by continuous stirring at 120 °C.

Preparation of a Stock Solution of Formamidinium-Oleate (FA-OL): In a typical synthesis, 521 mg of formamidinium acetate (5 mmol) was mixed with 20 mL of oleic acid (56 mmol). The resulting mixture was heated at 150 °C under stirring until the salt was completely dissolved.

Preparation of Lead Halide Stock Solution ($PbBr_2$): In a typical synthesis, the lead halide salt 345 mg of $PbBr_2$ (0.94 mmol) was added to a mixture of 2.5 mL of OLA, 2.5 mL of oleic, and 25 mL of 1-octadecene in a 50 mL sample vial. The resulting mixture was heated at 150 °C under continuous stirring until the salt was completely dissolved.

Synthesis of $CsPbBr_3$ Perovskite NCs (Stock Solution): In a typical synthesis, 6 mL of the $PbBr_2$ precursor solution was loaded in a 20 mL glass vial and it was heated on a hot plate until the temperature of the precursor solution reached 175 °C. Then, 400 µL of the pre-heated Cs-OL stock solution was swiftly injected into it under vigorous stirring (1 000 rpm). After 5 s, the vial cooled in an ice-water bath to quench the reaction. Subsequently, the thus obtained colloidal dispersion was purified without the use of antisolvent by centrifugation at 6 000 rpm for 10 min. The supernatant was discarded to remove the unreacted precursors and ligands and the sediment was redispersed in 1 mL of toluene. The colloidal dispersion was centrifuged again at 5 000 rpm for 8 min to remove the largest particles in the sediment.

Synthesis of $FAPbBr_3$ Perovskite NCs (Stock Solution): In a typical synthesis, 6 mL of the $PbBr_2$ precursor solution was loaded in a 20 mL glass vial and it was heated on a hot-plate until the temperature of the precursor solution reached 175 °C. Then, 2.5 mL of the pre-heated FA-OL stock solution was swiftly injected into it under vigorous stirring (1 000 rpm). After 5 s, the vial was removed from the hot-plate and placed in an ice-water bath to quench the reaction. $FAPbBr_3$The crude solution was purified without the use of antisolvent following the same procedure as described for $CsPbBr_3$.

Synthesis of $MAPbBr_3$ Perovskite NCs (Stock Solution): In a typical synthesis, lead oxide (44 mg), 2.5 mL of oleic acid, 0.025 mL of oleylamine, and 5 mL of octadecene were mixed in a 20 mL vial and dried under vacuum for 1 h at 125 °C. Then, the temperature was lowered to 65 °C under N_2. Subsequently, 170 µL of methylamine was injected, followed by the injection of a solution of benzoyl bromide (50 µL) in toluene (500 µL). After 5 s, the vial was removed from the hot plate and placed in an ice-water bath to quench the reaction. $MAPbBr_3$The crude solution was purified without the use of antisolvent following the same procedure as described for $CsPbBr_3$.

Note. In order to keep the same conditions in all the experiments described below, after the purification of the colloidal solutions, the absorption spectra of the samples were measured, and the concentration was adjusted (keeping the maximum concentration as possible) so that each solution had a similar optical density near the band edge.

Synthesis of $FA_xCs_{1-x}PbBr_3$ NCs by Interparticle A-Cation Exchange (Stock Solution): Mixed A-site cation NCs were obtained by interparticle A-site cation exchange reaction.[49] In a typical synthesis, colloidal solutions of $CsPbBr_3$ and $FAPbBr_3$ NCs dispersed in toluene were mixed in different ratios to produce the desired Cs/FA stoichiometry. Before mixing, the absorption spectra of the individual samples were measured, and the concentration was adjusted so that each solution had a similar optical density near the band edge. The mixture was kept stirring (500 rpm) for 5 min at room temperature and the reaction was monitored by photoluminescence spectroscopy.

Synthesis of $FA_xCs_{1-x}PbBr_3$ NCs by A-Cation Exchange (Stock Solution): Mixed A-site cation NCs were obtained by A-site exchange reaction in air conditions. In a typical synthesis, 1 mL of the FA-OL precursor solution was diluted in 9 mL of toluene to obtain a FA-OL solution ≈25 mM. To obtain the mixed A-site cation NCs, different volumes (0.1 – 1 mL) of the resulting FA-OL solution 25 mM were added to 1 mL of $CsPbBr_3$ NCs stock solution. The solution was kept under stirring (500 rpm) for 5 min at room temperature and the reaction was monitored by photoluminescence spectroscopy to confirm the A-site cation exchange.

Washing with Antisolvents: The washing process was performed systematically for the different A-site cation compositions. In each cycle of washing, certain volume of the different stock solutions was mixed with MeOAc (antisolvent) keeping always a constant volume ratio (2:1). After the addition of the antisolvent, the solutions became turbid and they were centrifuged at 6 000 rpm, 5 min. The supernatant was discarded, and the sediment was redispersed in toluene using the same starting volume.

Optical Characterization: UV–vis extinction spectra were carried out using a Cary-60 UV–vis spectrophotometer (Agilent). Photoluminescence spectra were obtained with a Cary Eclipse Fluorescence Spectrophotometer (Agilent). Time-resolved photoluminescence spectra were obtained using a FluoroMax-3 (Horiba Jobin Yvon) spectrophotometer and the PL decay traces were measured by exciting the samples at 287 nm using <1.2 ns laser diode. Quantum yield measurements were acquired using a calibrated integrating sphere with a spectrophotometer JASCO FP-8550 using an excitation wavelength $\lambda ex = 350$ nm for all of the measurements. All solutions were diluted to an optical density of 0.1 or lower at the excitation wavelength in order to minimize the reabsorption of the fluorophore.

Quartz cuvettes with an optical path length of 1 cm were used for all optical analyses.

Transmission Electron Microscopy (TEM) Characterization: Transmission electron microscopy (TEM) images were obtained with a JEOL JEM 1010 transmission electron microscope operating at an acceleration voltage of 100 kV.

Nuclear Magnetic Resonance (NMR) Characterization: NMR measurements were performed at 298 K, on a Bruker Avance III 600 MHz (600.13 MHz) spectrometer, equipped with a 5 mm QCI cryoprobe. Before each acquisition, matching and tuning and, resolution, were automatically adjusted, the 90° pulse was calculated on each tube by using Bruker's automatic routines.[62] ^{1}H NMR spectra in toluene-D were recorded with 128 scans, without dunny scan, by using 65 536 digit points, a relaxation delay of 30 s, over a spectral width of 20.83 ppm with the offset at 6.18 ppm.

^{1}H quantitative NMR spectra for PULCON method in DMSO were recorded with 32 transients without dunny scans, 65 536 points of digitalization, 30 s of inter pulses delay, over a spectral width of 20.83 ppm with offset at 6.18 ppm. An exponential apodization function of 0.3 Hz was applied to FIDs to smooth the noise, prior to the Fourier transform to be applied. ^{1}H NMR spectra were manually phased and automatically baseline corrected.

2D ^{1}H–^{1}H NOESY experiments in toluene-d_8 were recorded after 32 dunny scans, by accumulating 16 transients, with 2048 digits and 256 increments, with 300 ms of mixing time, over a spectral width of 15 ppm (offset at 7.49 ppm).

Sample Preparation: For the NMR characterization, the different A-site cation samples washed 2 times with MeOAc were then dried and redispersed in deuterated toluene (500 µL). 5 mm sampleJet tubes were used for NMR measurement. The colloidal solution was loaded into a 5 mm disposable sample Jet tubes. For the ligand quantification, the colloidal solutions already characterized in deuterated toluene, where dried using a N2 flow, and the resulting material was dissolved in deuterated DMSO (200 µL) and loaded into a 3 mm disposable sampleJet tube.

Ligand Quantification: The concentration of both ligands ([OLAm & OL]) was quantified using quantitative NMR spectrum, by comparing the integrated peak intensity of ligand signals, each normalized for the number of protons generating the peak (2H), to that of standard external solution of dimethylsulfone (5 mM, TraceCERT) in DMSO-d_6, the latter normalized to 6 H. The concentration of OLAm was obtained selectively by the integrated peak ratio between the pseudo triplet at 2.75 ppm to that of external standard solution through the PULCON (PUlse Length-based CONcentration determination) method.[44] Whereas the OL concentration was calculated by difference, measuring directly with PULCON the concentration of all the species containing the double bound (signal at 5.3 ppm), that is, both OLAm and OL and subtracting to that value the concentration of OLAm previously measured (signal at 2.75p pm), according to the following formula:

$$\left([OL]_{calc} = [OLAm + OL]_{measured\ by\ PULCON} - [OLAm]_{measured\ by\ PULCON}\right) \quad (1)$$

Inductively Coupled Plasma–Optical Emission Spectroscopy (ICP-OES): After the ligand quantification, the Pb concentration of the NCs dissolved in deuterated DMSO was obtained by ICP-OES on an aiCAP 6000 spectrometer (Thermo Scientific). Prior the measurement, 50 µL of the DMSO – d_6 sample were diluted to 10 mL in an aqueous solution of aqua regia (1:10) and subjected to an acid digestion overnight.

Ligand density: The ligand density of the samples was obtained by calculating the ratio of the ligand concentration and NC surface in the DMSO-d_6 solution:

$$Ligand\ density\ \left(nm^{-2}\right) = Ligands\ per\ NC / NC\ surface\ \left(nm^2\right) \quad (2)$$

The total NC surface was determined through the Pb concentration in the DMSO-d_6 sample and the size distribution of the NCs considering a unit cell size of 0.589 nm:

$$NC\ surface\ \left(nm^2\right) = [NC\ size\ (nm)]\,2 \times 6 \quad (3)$$

$$Ligands\ per\ NC = total\ ligands\ concentration\ \left(mmol/mL^{-1}\right) / NC\ concentration\ \left(mmol/mL^{-1}\right) \quad (4)$$

$$NC\ concentration(mL^{-1}) = \left(\frac{Total\ concetration\ of\ Pb(mL^{-1})}{Pb\ atoms/NC}\right) \quad (5)$$

$$Pb\ atoms/NC = \left[\frac{NC\ size\ (nm)}{0.589\ nm/unit\ cell}\right]^3 \quad (6)$$

X-Ray Photoemission Spectroscopy: The samples were prepared by drop-casting 200 µL NC solutions (similar concentration) onto spectroscopic glass substrates inside an N_2-filled glovebox. Then the dried films were sent for XPS measurement. XPS data was acquired using a Kratos Axis SUPRA using monochromated Al Kα (1 486.69 eV) Xrays at 12 mA emission and 15 kV HT (180 W), with an analysis area of 700 µm × 300 µm. The instrument was calibrated to the gold metal Au 4f core level (83.95 eV) and dispersion-adjusted to give a binding energy (BE) of 932.6 eV for the Cu 2p3/2 line of metallic copper. Ag 3d5/2 line FWHM at 10 eV pass energy was 0.544 eV. The source resolution for monochromatic Al Kα X-rays is ≈0.3 eV. The instrumental resolution was determined to be 0.29 at 10 eV pass energy using the Fermi edge of the valence band for metallic silver. The resolution with the charge compensation system was <1.33 eV FWHM on PTFE. High-resolution spectra were obtained using a pass energy of 20 eV, step size of 0.1 eV, and sweep time of 60 s, resulting in a line width of 0.696 eV for Au 4f7/2. Survey spectra were obtained using a pass energy of 160 eV. Charge neutralization was achieved using an electron flood gun with a filament current of 0.38 A, a charge balance of 2 V, and a filament bias of 4.2 V. Successful neutralization was adjudged by analyzing the C 1s region wherein a sharp peak with no lower BE structure was obtained. The spectra were charged and corrected to the main line of the carbon 1s spectrum (adventitious carbon) set to 284.8 eV. All data was recorded at a base pressure of below 9×10^{-9} Torr and at room temperature (294 K). Data was analyzed using the software CasaXPS v2.3.18PR1.0.

X-Ray Diffraction: XRD analysis was performed on a PANanalytical Empyrean X-ray diffractometer, equipped with a 1.8 kW Cu Kα ceramic anode and a PIXcel3D 2 × 2 area detector, operating at 45 kV and 40 mA. The samples were analyzed in the form of dried powders on a silicon substrate prepared after washing them previously with MeOAc between once and three times.

Supporting Information

Supporting Information is available from the Wiley Online Library or from the author.

Acknowledgements

C.O.M. and J.Y. contributed equally to this work. C.O.M. acknowledges the support from the Xunta de Galicia through PhD fellowship (ED481A-2021/318). L.P. acknowledges support from the Spanish Ministerio de Ciencia e Innovación through Ramón y Cajal grant (grant no. RYC2018-026103-I), the Spanish State Research Agency (grant nos. PID2020-117371RA-I00 and TED2021-131628A-I00), and a grant from the Xunta de Galicia (grant no. ED431F2021/05). J.Y. and R.L.Z.H. acknowledge support from a UK Research and Innovation (UKRI) Frontier Grant (no. EP/X029900/1), awarded via the European Research Council Starting Grant 2021 scheme. J.Y. also gives thanks to the Cambridge Philosophical Society for a Research Studentship Grant. R.L.Z.H. thanks the Royal Academy of Engineering through the Research Fellowships scheme (no. RF\201718\17101), as well as the Centre of Advanced Materials for Integrated Energy Systems (CAM-IES; EPSRC grant no. EP/T012218/1). The authors acknowledge the Universidad de Vigo/CSIUG for open accessfunding. XPS data was acquired at the EPSRC National Facility for XPS ("HarwellXPS", EPSRC grant no: EP/Y023587/1, EP/Y023609/1, EP/Y023536/1, EP/Y023552/1 and EP/Y023544/1). We acknowledge Dr. Mark Isaacs for obtaining the XPS data.

Conflict of Interest

The authors declare no conflict of interest.

Data Availability Statement

The data that support the findings of this study are available from the corresponding author upon reasonable request.

Keywords

mixed A-site cation perovskites, nanocrystal purification, perovskite nanocrystals, surface chemistry, surface defects

Received: April 14, 2024
Published online:

[1] A. Dey, J. Ye, A. De, E. Debroye, S. K. Ha, E. Bladt, A. S. Kshirsagar, Z. Wang, J. Yin, Y. Wang, L. N. Quan, F. Yan, M. Gao, X. Li, J. Shamsi, T. Debnath, M. Cao, M. A. Scheel, S. Kumar, J. A. Steele, M. Gerhard, L. Chouhan, K. Xu, X.-G. Wu, Y. Li, Y. Zhang, A. Dutta, C. Han, I. Vincon, A. L. Rogach, *ACS Nano* **2021**, *15*, 10775.
[2] M. Imran, V. Caligiuri, M. Wang, L. Goldoni, M. Prato, R. Krahne, L. De Trizio, L. Manna, *J. Am. Chem. Soc.* **2018**, *140*, 2656.
[3] S. Wang, A. A. Yousefi Amin, L. Wu, M. Cao, Q. Zhang, T. Ameri, *Small Struct.* **2021**, *2*, 2000124.
[4] H. Dong, C. Ran, W. Gao, M. Li, Y. Xia, W. Huang, *eLight* **2023**, *3*, 3.
[5] N. Zhou, D. Wang, Y. Bao, R. Zhu, P. Yang, L. Song, *Adv. Optical Mater.* **2023**, *11*, 2202681.
[6] L. Liu, A. Najar, K. Wang, M. Du, S. Liu, *Adv. Sci.* **2022**, *9*, 2104577.
[7] J. Y. Kim, J.-W. Lee, H. S. Jung, H. Shin, N.-G. Park, *Chem. Rev.* **2020**, *120*, 7867.
[8] N. Livakas, S. Toso, Y. P. Ivanov, T. Das, S. Chakraborty, G. Divitini, L. Manna, *J. Am. Chem. Soc.* **2023**, *145*, 20442.
[9] R. Grisorio, M. E. Di Clemente, E. Fanizza, I. Allegretta, D. Altamura, M. Striccoli, R. Terzano, C. Giannini, M. Irimia-Vladu, G. P. Suranna, *Nanoscale* **2019**, *11*, 986.
[10] S. R. Smock, Y. Chen, A. J. Rossini, R. L. Brutchey, *Acc. Chem. Res.* **2021**, *54*, 707.
[11] J. De Roo, M. Ibáñez, P. Geiregat, G. Nedelcu, W. Walravens, J. Maes, J. C. Martins, I. Van Driessche, M. V. Kovalenko, Z. Hens, *ACS Nano* **2016**, *10*, 2071.
[12] N. Fiuza-Maneiro, K. Sun, I. López-Fernández, S. Gómez-Graña, P. Müller-Buschbaum, L. Polavarapu, *ACS Energy Lett.* **2023**, *8*, 1152.
[13] S. Mourdikoudis, M. Menelaou, N. Fiuza-Maneiro, G. Zheng, S. Wei, J. Pérez-Juste, L. Polavarapu, Z. Sofer, *Nanoscale Horiz.* **2022**, *7*, 941.
[14] M. Kazes, T. Udayabhaskararao, S. Dey, D. Oron, *Acc. Chem. Res.* **2021**, *54*, 1409.
[15] K. Hills-Kimball, H. Yang, T. Cai, J. Wang, O. Chen, *Adv. Sci.* **2021**, *8*, 2100214.
[16] A. Stelmakh, M. Aebli, A. Baumketner, M. V. Kovalenko, *Chem. Mater.* **2021**, *33*, 5962.
[17] F. Zaccaria, B. Zhang, L. Goldoni, M. Imran, J. Zito, B. van Beek, S. Lauciello, L. De Trizio, L. Manna, I. Infante, *ACS Nano* **2022**, *16*, 1444.
[18] L. De Trizio, I. Infante, L. Manna, *Acc. Chem. Res.* **2023**, *56*, 1815.
[19] V. K. Ravi, P. K. Santra, N. Joshi, J. Chugh, S. K. Singh, H. Rensmo, P. Ghosh, A. Nag, *J. Phys. Chem. Lett.* **2017**, *8*, 4988.
[20] A. Swarnkar, A. R. Marshall, E. M. Sanehira, B. D. Chernomordik, D. T. Moore, J. A. Christians, T. Chakrabarti, J. M. Luther, *Science* **2016**, *354*, 92.
[21] M. De Franco, M. Cirignano, T. Cavattoni, H. Bahmani Jalali, M. Prato, F. Di Stasio, *Optical Mater.: X* **2022**, *13*, 100124.

[22] L. C. Chen, C. H. Tien, P. W. Tseng, Z. L. Tseng, W. L. Huang, Y. X. Xu, H. C. Kuo, *IEEE Access* **2020**, *8*, 159415.
[23] J. Ye, Z. Li, D. J. Kubicki, Y. Zhang, L. Dai, C. Otero-Martínez, M. A. Reus, R. Arul, K. R. Dudipala, Z. Andaji-Garmaroudi, Y.-T. Huang, Z. Li, Z. Chen, P. Müller-Buschbaum, H.-L. Yip, S. D. Stranks, C. P. Grey, J. J. Baumberg, N. C. Greenham, L. Polavarapu, A. Rao, R. L. Z. Hoye, *J. Am. Chem. Soc.* **2022**, *144*, 12102.
[24] Q. Jing, M. Zhang, X. Huang, X. Ren, P. Wang, Z. Lu, *Nanoscale* **2017**, *9*, 7391.
[25] K. Hoshi, T. Chiba, J. Sato, Y. Hayashi, Y. Takahashi, H. Ebe, S. Ohisa, J. Kido, *ACS Appl. Mater. Interfaces* **2018**, *10*, 24607.
[26] J. Xue, J.-W. Lee, Z. Dai, R. Wang, S. Nuryyeva, M. E. Liao, S.-Y. Chang, L. Meng, D. Meng, P. Sun, O. Lin, M. S. Goorsky, Y. Yang, *Joule* **2018**, *2*, 1866.
[27] Y. Zhang, T. D. Siegler, C. J. Thomas, M. K. Abney, T. Shah, A. De Gorostiza, R. M. Greene, B. A. Korgel, *Chem. Mater.* **2020**, *32*, 5410.
[28] Y. Hassan, J. H. Park, M. L. Crawford, A. Sadhanala, J. Lee, J. C. Sadighian, E. Mosconi, R. Shivanna, E. Radicchi, M. Jeong, C. Yang, H. Choi, S. H. Park, M. H. Song, F. De Angelis, C. Y. Wong, R. H. Friend, B. R. Lee, H. J. Snaith, *Nature* **2021**, *591*, 72.
[29] J. Ye, M. M. Byranvand, C. O. Martínez, R. L. Z. Hoye, M. Saliba, L. Polavarapu, *Angew. Chem., Int. Ed.* **2021**, *60*, 21636.
[30] F. Krieg, Q. K. Ong, M. Burian, G. Rainò, D. Naumenko, H. Amenitsch, A. Süess, M. J. Grotevent, F. Krumeich, M. I. Bodnarchuk, I. Shorubalko, F. Stellacci, M. V. Kovalenko, *J. Am. Chem. Soc.* **2019**, *141*, 19839.
[31] S. Wang, W. Wang, S. Donmez, Y. Xin, H. Mattoussi, *Chem. Mater.* **2022**, *34*, 4924.
[32] X. Y. Zhu, V. Podzorov, *J. Phys. Chem. Lett.* **2015**, *6*, 4758.
[33] F. Zheng, L. Wang, *Energy Environ. Sci.* **2019**, *12*, 1219.
[34] Z. Yang, J. Song, H. Zeng, M. Wang, *Mater. Today Energy* **2019**, *14*, 100338.
[35] M. M. Byranvand, C. Otero-Martínez, J. Ye, W. Zuo, L. Manna, M. Saliba, R. L. Z. Hoye, L. Polavarapu, *Adv. Opt. Mater.* **2022**, *10*, 2200423.
[36] D. Jia, J. Chen, R. Zhuang, Y. Hua, X. Zhang, *Adv. Mater.* **2023**, *35*, 2212160.
[37] J. Yuan, A. Hazarika, Q. Zhao, X. Ling, T. Moot, W. Ma, J. M. Luther, *Joule* **2020**, *4*, 1160.
[38] I. López-Fernández, D. Valli, C.-Y. Wang, S. Samanta, T. Okamoto, Y.-T. Huang, K. Sun, Y. Liu, V. S. Chirvony, A. Patra, J. Zito, L. De Trizio, D. Gaur, H.-T. Sun, Z. Xia, X. Li, H. Zeng, I. Mora-Seró, N. Pradhan, J. P. Martínez-Pastor, P. Müller-Buschbaum, V. Biju, T. Debnath, M. Saliba, E. Debroye, R. L. Z. Hoye, I. Infante, L. Manna, L. Polavarapu, *Adv. Funct. Mater.* **2024**, *34*, 2307896.
[39] M. V. Kovalenko, L. Protesescu, M. I. Bodnarchuk, *Science* **2017**, *358*, 745.
[40] L. Protesescu, S. Yakunin, M. I. Bodnarchuk, F. Krieg, R. Caputo, C. H. Hendon, R. X. Yang, A. Walsh, M. V. Kovalenko, *Nano Lett.* **2015**, *15*, 3692.
[41] A. Hazarika, Q. Zhao, E. A. Gaulding, J. A. Christians, B. Dou, A. R. Marshall, T. Moot, J. J. Berry, J. C. Johnson, J. M. Luther, *ACS Nano* **2018**, *12*, 10327.
[42] S. R. Smock, T. J. Williams, R. L. Brutchey, *Angew. Chem., Int. Ed.* **2018**, *57*, 11711.
[43] Z. Liu, R. Pascazio, L. Goldoni, D. Maggioni, D. Zhu, Y. P. Ivanov, G. Divitini, J. L. Camarelles, H. B. Jalali, I. Infante, L. De Trizio, L. Manna, *J. Am. Chem. Soc.* **2023**, *145*, 18329.
[44] G. Wider, L. Dreier, *J. Am. Chem. Soc.* **2006**, *128*, 2571.
[45] H. Huang, M. I. Bodnarchuk, S. V. Kershaw, M. V. Kovalenko, A. L. Rogach, *ACS Energy Lett.* **2017**, *2*, 2071.
[46] C. Otero-Martínez, M. Imran, N. J. Schrenker, J. Ye, K. Ji, A. Rao, S. D. Stranks, R. L. Z. Hoye, S. Bals, L. Manna, J. Pérez-Juste, L. Polavarapu, *Angew. Chem., Int. Ed.* **2022**, *61*, 202205617.
[47] M. Imran, P. Ijaz, L. Goldoni, D. Maggioni, U. Petralanda, M. Prato, G. Almeida, I. Infante, L. Manna, *ACS Energy Lett.* **2019**, *4*, 819.
[48] F. Krieg, S. T. Ochsenbein, S. Yakunin, S. ten Brinck, P. Aellen, A. Süess, B. Clerc, D. Guggisberg, O. Nazarenko, Y. Shynkarenko, S. Kumar, C.-J. Shih, I. Infante, M. V. Kovalenko, *ACS Energy Lett.* **2018**, *3*, 641.
[49] J. Pan, Y. Shang, J. Yin, M. De Bastiani, W. Peng, I. Dursun, L. Sinatra, A. M. El-Zohry, M. N. Hedhili, A.-H. Emwas, O. F. Mohammed, Z. Ning, O. M. Bakr, *J. Am. Chem. Soc.* **2018**, *140*, 562.
[50] Y. Tan, Y. Zou, L. Wu, Q. Huang, D. Yang, M. Chen, M. Ban, C. Wu, T. Wu, S. Bai, T. Song, Q. Zhang, B. Sun, *ACS Appl. Mater. Interfaces* **2018**, *10*, 3784.
[51] T. Chiba, S. Ishikawa, J. Sato, Y. Takahashi, H. Ebe, S. Ohisa, J. Kido, *Adv. Opt. Mater.* **2020**, *8*, 2000289.
[52] S. Wang, L. Du, Z. Jin, Y. Xin, H. Mattoussi, *J. Am. Chem. Soc.* **2020**, *142*, 12669.
[53] W. Yin, M. Li, W. Dong, Z. Luo, Y. Li, J. Qian, J. Zhang, W. Zhang, Y. Zhang, S. V. Kershaw, X. Zhang, W. Zheng, A. L. Rogach, *ACS Energy Lett.* **2021**, *6*, 477.
[54] C.-H. Kuan, S.-H. Yang, *Mater. Adv.* **2022**, *3*, 7824.
[55] Y. Zhang, G. Hou, Y. Wu, M. Chen, Y. Dai, S. Liu, Q. Zhao, H. Lin, J. Fang, C. Jing, J. Chu, *Langmuir* **2023**, *39*, 6222.
[56] Y. Zhang, G. Li, G. Hou, J. Lin, M. Chen, S. Liu, H. Lin, J. Fang, C. Jing, J. Chu, *Chem. Eng. J.* **2022**, *438*, 135270.
[57] M. Yu, D. Zhang, Y. Xu, J. Lin, C. Yu, Y. Fang, Z. Liu, Z. Guo, C. Tang, Y. Huang, *J. Colloid Interface Sci.* **2022**, *608*, 2367.
[58] L. Zhang, Q. Zhang, X. Xing, Y. Jiang, T. He, Y. Huang, Z. Ma, J. Yang, M. Yuan, *ChemNanoMat* **2019**, *5*, 318.
[59] C. Zhang, S. Wang, X. Li, M. Yuan, L. Turyanska, X. Yang, *Adv. Funct. Mater.* **2020**, *30*, 1910582.
[60] C. C. Stoumpos, C. D. Malliakas, J. A. Peters, Z. Liu, M. Sebastian, J. Im, T. C. Chasapis, A. C. Wibowo, D. Y. Chung, A. J. Freeman, B. W. Wessels, M. G. Kanatzidis, *Cryst. Growth Des.* **2013**, *13*, 2722.
[61] L. Protesescu, S. Yakunin, M. I. Bodnarchuk, F. Bertolotti, N. Masciocchi, A. Guagliardi, M. V. Kovalenko, *J. Am. Chem. Soc.* **2016**, *138*, 14202.
[62] P. S. C. Wu, G. Otting, *J. Magn. Reson.* **2005**, *176*, 115.